Limnol. Oceanogr., 59(6), 2014, 2133–2149

doi:10.4319/lo.2014.59.6.2133

Proxies of community production derived from the diel variability of particulate attenuation and backscattering coefficients in the northwest Mediterranean Sea

Morvan Barnes [1,2] and David Antoine [1,2,3,*]

[1] Sorbonne Universités, Université Pierre et Marie Curie, Laboratoire d'Océanographie de Villefranche, Observatoire Océanologique, Villefranche-sur-Mer, France

[2] Centre National de la Recherche (CNRS), Laboratoire d'Océanographie de Villefranche, Observatoire Océanologique, Villefranche-sur-Mer, France

[3] Department of Imaging and Applied Physics, Remote Sensing and Satellite Research Group, Curtin University, Perth, Australia

Abstract

A 6 yr time series of high frequency inherent optical property (IOP) measurements in the Mediterranean was used to derive information on the diel and seasonal variability of particulate production. Empirical relationships between particulate attenuation (c_p), particulate backscattering (b_{bp}), and particulate organic carbon allowed calculation of estimates of net community production (NCP), daytime NCP (NCPd), and gross community production (GCP) from the diel variations in either IOP. Similar seasonal variations and good correlation ($r = 0.83$, $p < 0.001$) between daily means of c_p and b_{bp} were observed, yet differences in the timing and amplitude of their diel cycles led to significant differences in their derived production metrics. Best agreement was obtained during bloom proliferation (44.1–66.7% shared variance) when all three production estimates were highest, while worst was during bloom decline. Best overall correlation was found for NCPd. Accordingly, only c_p-derived estimates reproduced predicted seasonal variations in community production and seasonality of "traditional" chlorophyll-based primary production models. Analysis of the diel cycles of "real-time" net community production (NCPh), determined from the first-derivative of either c_p or b_{bp}, revealed ca. fourfold to eightfold lower daytime NCPh, twofold to fivefold lower daily maximum NCPh, and twice as much intraseasonal variability relative to the mean amplitude of diel variations for b_{bp}. Although the timing of maximum of c_p-derived NCPh was consistently prior to solar noon, significant seasonal differences in the timing of maximum b_{bp}-derived NCPh was observed. Particulate backscattering may be used to infer biogeochemical properties, while greater understanding of the diel cycles of b_{bp} is needed before b_{bp} can be used to investigate daily community production.

Ocean particle dynamics confer essential information regarding biogeochemical processes at a wide range of temporal and spatial scales (Stramski et al. 1999; Oubelkheir et al. 2005; Dall'Olmo et al. 2012). Inherent optical properties (IOPs) of oceanic waters, such as the particulate beam attenuation coefficient (c_p) and the particulate backscattering coefficient (b_{bp}), have increasingly been used to investigate oceanic biogeochemical processes, to investigate phytoplankton dynamics, and to reduce uncertainties associated with carbon budgets (Sosik 2008). Development of nonintrusive instrumentation with a high ratio of data output to measurement effort has rendered optical sensors an attractive proposition for biogeochemical analyses. Empirical bio-optical relationships between IOPs and biogeochemical parameters have thus enabled higher resolution determinations of Case 1 biogeochemical variability from field measurements or remote sensing observations (Cetinic et al. 2012). These optical proxies have enabled measurements of particulate organic carbon (POC) at higher temporal and spatial scales than are attainable with traditional discrete water sampling methods. Such data would allow us to overcome current limitations of a biogeochemically undersampled ocean (Claustre et al. 2010).

The particulate beam attenuation coefficient is defined as the sum of particulate absorption and scattering and can be considered an optical measure of the particulate pool. It is most sensitive to particles between 0.5 and 20 μm (Stramski and Kiefer 1991). It is now recognized as a useful proxy of POC concentration (Loisel and Morel 1998; Claustre et al. 1999). Observations of c_p variability have increased in recent years, including in the Mediterranean Sea (Oubelkheir and Sciandra 2008; Gernez et al. 2011). In comparison, the variability in particulate backscattering is less well known and poorly constrained (Antoine et al. 2011) despite b_{bp} showing closer affinity to remote sensing observations. The co-variability of b_{bp} and POC (Boss et al. 2004; Cetinic et al. 2012) or phytoplankton chlorophyll *a* (Martinez-Vicente et al. 2012) suggests that b_{bp} may also be a useful proxy for biogeochemical properties. Indeed b_{bp} and c_p show strong coherence across different environments (Westberry et al. 2010) despite the disputed role of phytoplankton in determining b_{bp} (Stramski et al. 2004). Several methods have been proposed for estimating higher biogeochemical quantities, such as ecophysiological rates and community carbon production from c_p (Gernez et al. 2011; Dall'Olmo et al. 2012), but whether these work for b_{bp} is yet to be shown.

Our understanding of the long-term spatiotemporal variability of the global particulate pool has improved markedly since the advent of remote sensing (Vantrepotte

* Corresponding author: david.antoine@curtin.edu.au

et al. 2011) and has highlighted the possible effects of climate oscillations on oceanic biology (Martinez et al. 2009). Yet our knowledge of smaller scale temporal variability is very limited, and recent efforts have sought to extend our understanding of diurnal variability of the particulate pool (Gernez et al. 2011; Loisel et al. 2011; Dall'Olmo et al. 2012). Diel variability of optical properties is a well-established phenomenon, resulting from cyclic solar forcing and upper mixed layer dynamics. However, the potential underlying mechanical causes are numerous and remain poorly understood. The diurnal c_p increase is related to photosynthetic organic production by phytoplankton (Siegel et al. 1989) and the associated increase in particle size and/or refractive index (Stramski and Reynolds 1993), as well as changes in phytoplankton type, physiology, and general community composition (Claustre et al. 2008; Oubelkheir and Sciandra 2008). The development of autonomous moored instruments provides novel opportunities to characterize diel variability over long temporal periods.

In this study, we make use of a 6 yr time series (2006–2011) of near continuous (every 15 min) optical measurements performed at the Bouée pour l'acquisition de séries optiques à long terme (BOUSSOLE) site in the northwestern Mediterranean Sea (Antoine et al. 2006, 2008). This builds on the work of Gernez et al. (2011) who used 2 yr of BOUSSOLE c_p data to examine seasonal variations in c_p-derived community production. Here, the different temporal scales of variability (from annual to diel) of c_p and b_{bp} are characterized and compared under varying environmental conditions. Relationships between biogeochemical variables are investigated under different trophic conditions. In a second step, the use of both c_p and b_{bp} toward the derivation of several community production related quantities is explored. Finally, the full diel cycles of net community production are analyzed and related to phytoplankton dynamics and their responses to environmental conditions.

Methods

Sampling strategy—The BOUSSOLE site is situated in Case 1 waters of the Ligurian Sea in the northwestern Mediterranean Sea (Fig. 1). The westward flowing Ligurian current dominates the physical advection, while the site shows marked seasonality in physical characteristics. Deep mixed layers (usually down to 400 m; occasionally > 1000 m) are consistently present during winter, whereas marked stratification occurs throughout summer. The onset of stratification between February and March is accompanied by a prominent spring bloom which is followed by marked oligotrophy.

To capture the concomitant variability in optical properties, an autonomous moored platform, operating in quasi-continuous mode, has been deployed at the BOUSSOLE site since September 2003. The platform measures radiometric quantities at two depths (4 and 9 m) as well as above the surface. Data acquisition occurs every 15 min and is represented by median data from 1 min long acquisitions. Two sister buoys are used with ca. 6 month

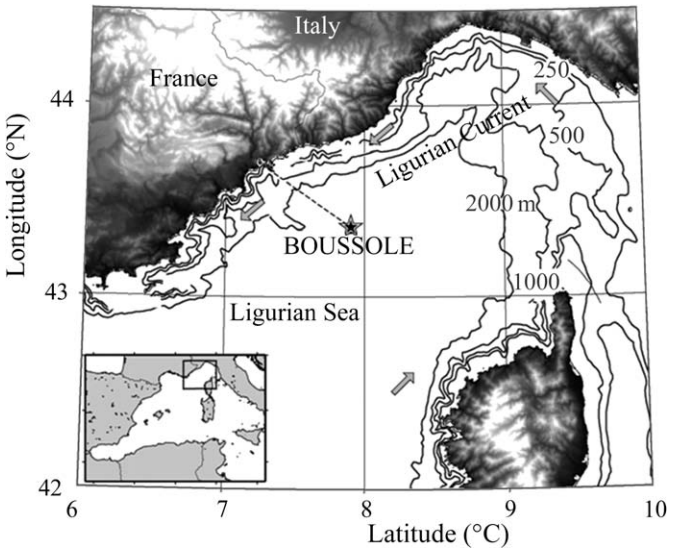

Fig. 1. Regional map situating the BOUSSOLE site in the Ligurian Sea (northwestern Mediterranean).

rotations to permit calibration checks and serviced every month. Excessive biofouling is prevented by regular cleaning performed by divers every 2–4 weeks and by the use of copper and antifouling paint wherever possible on all instruments. Comparisons of data before and after cleaning allow for further quality controls resulting in the elimination of possibly corrupt observations. Monthly 0–400 m downcasts are also performed for acquisition of hydrological data including conductivity, temperature, and depth (CTD) measurements of temperature, complementary c_p measurements, discrete phytoplankton pigment analyses, and particulate absorption measurements. Optical measurements used here are the particulate beam attenuation coefficient c_p, the backscattering coefficient b_{bp}, and the photosynthetically available radiation (PAR).

Optical measurements—The transmittance (*Tr*, %) was measured at 660 nm with 25 cm pathlength Wetlabs C-star transmissometers (acceptance angle of 1.2°). At this wavelength the absorption of colored dissolved organic matter is assumed to be negligible (Bricaud et al. 1981). The particulate beam attenuation coefficient c_p was then calculated as

$$c_p(660) = -\frac{1}{0.25}\ln\left(\frac{Tr}{100}\right)$$

Deployment length of each instrument on the BOUSSOLE buoy was between 4 and 12 months, and monthly CTD measurements of c_p were taken to 400 m depth. Three moored instruments were used across the time series, and each was factory calibrated before each deployment (with annual calibration for the CTD instrument) with deionized, ultrafiltered, ultraviolet screened water. Air and blocked beam calibrations were also checked prior to deployment. In situ dark measurements, where the beam is blocked by black neoprene covers, were used to check for significant deviation (but not to induce corrections). To harmonize the

c_p time series acquired with different instruments, the CTD measurements at 4 and 9 m were used as a reference, resulting in the removal of a fixed or variable bias from each deployment. Prior to CTD casts, instrument windows were cleaned with a few drops of methanol and optical lens paper, and a short 50 m cast is undertaken to wash the CTD–rosette system. Drift of the CTD measurements was corrected for using bottom data (average between 375–400 m), which are usually occupied by low particle concentration Levantine water (Oubelkheir et al. 2005) such that mean c_p at these depths equaled 0.055 m^{-1}.

The backscattering coefficient is calculated at 555 nm from the volume scattering function at 140° $\beta(140)$, measured using two hydro-optics, biology, and instrumentation laboratories (HOBI Labs) Hydroscat-2 and, from October 2007, two Hydroscat-4 backscattering meters. Instruments are calibrated before and after each deployment following Maffione and Dana (1997), while dark measurements are performed in situ using black neoprene cap. Instruments operate at 1 Hz so that 60 measurements are collected during each of the 1 min acquisition sequences, the median of which is used as a representative value for $\beta(140)$. We calculated b_{bp} following Maffione and Dana (1997):

$$b_{bp} = 2\pi\chi_p(\beta(140) - \beta_w(140))$$

where $\chi_p = 1.13$ and $\beta_w(140)$ is computed following Zhang et al. (2009) based on temperature and salinity measurements and corrected for pathlength attenuation following Maffione and Dana (1997) using the beam attenuation coefficient, the total absorption coefficient derived from the inversion of the diffuse attenuation coefficient for downward irradiance (Kd) and the irradiance reflectance (R; *see* eqs. 12 and 13 in Morel et al. 2006). Above-water photosynthetically available radiation (PAR between 400 and 700 nm; μmol photons m^{-2} s^{-1}) was estimated by fitting the solar irradiance model of Gregg and Carder (1990) to seven discrete irradiance values measured by a seven band Satlantic OCI-200 radiometer mounted on top of the buoy.

Phytoplankton pigments—Water samples for phytoplankton pigments were collected monthly at 11 depths from 5 to 200 m using Niskin bottles. Samples at 5 and 10 m are used here. Seawater was filtered through 25 mm GF/F filters (0.7 μm porosity), stored in liquid nitrogen, and subsequently analyzed for phytoplankton pigments using high-performance liquid chromatography following Ras et al. (2008). A continuous record of mean daily chlorophyll *a* (Chl *a*) was generated by supplementing these data with those from ocean color sensors following Antoine et al. (2008).

Physical dynamics—Water temperature (°C) and salinity were measured with a Sea-Bird Electronics (SBE) 37-SI CTD installed at 9 m depth. Monthly vertical temperature and salinity profiles were performed using a SBE 911+ CTD equipped with a Digiquartz Paroscientific pressure sensor and SBE 3 and SBE 4 temperature and conductivity sensors. Mixed layer depth (z_m) was determined using a density gradient criterion of 0.125 kg m^{-3} (Levitus 1982). Wind speed was measured on an hourly basis by a weather buoy two nautical miles from BOUSSOLE operated by Météo France. With our goal to characterize diel variations at BOUSSOLE, it was necessary to eliminate from consideration data where changes in optical properties could be due to strong horizontal or vertical advection. Days were selected for analysis only if sea surface temperature, salinity, buoy depth, and wind speed remained reasonably stable as documented by Gernez et al. (2011).

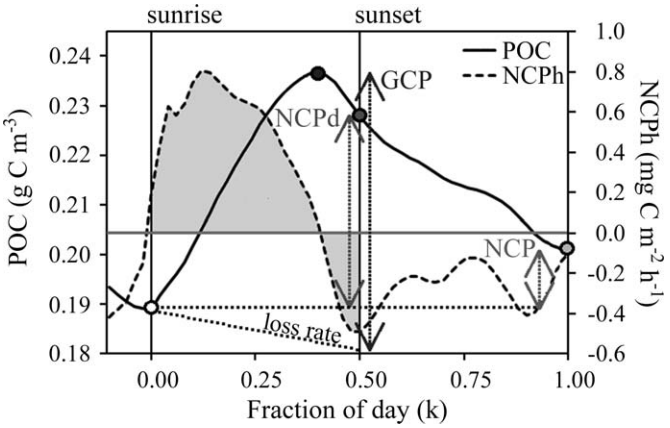

Fig. 2. Example of a diel cycle of POC (thick line) and NCPh (dashed line) plotted against the fraction of day (k). Particulate organic carbon at sunrise (k = 0) and at sunset (k = 0.5) are indicated, as well as the maximum value. The horizontal dotted line shows the sunrise minimum POC. Net community production (NCP; g C m^{-2} d^{-1}), daytime NCP (NCPd; g C m^{-2} d^{-1}), and gross community production (GCP; g C m^{-2} d^{-1}) are indicated.

Characterization of diel variability in IOPs—The amplitude of diel variation in c_p (m^{-1}) and b_{bp} (m^{-1}; Δc_p and Δb_{bp}, respectively) was determined as the difference between sunset and sunrise values (± 30 min averaged values) and are thus not necessarily the maximum diurnal change. Fractions of the day (*k*) are used, rather than hours, in order to allow comparison between days of varying photoperiod whereby *k* at sunrise, noon, sunset, and the next sunrise correspond to $k = 0$, 0.25, 0.5, and 1.

Net community and primary production—Particulate organic carbon (POC) was estimated from c_p and b_{bp} following empirical linear relationships established for the Mediterranean by Oubelkheir and Sciandra (2008; 1.78 m^2 g C^{-1}) and Loisel et al. (2001; 0.0266 m^2 g C^{-1}), respectively. Exact determination of net community production (NCP) cannot be derived from the diel changes in c_p or b_{bp}; only proxies of NCP or similar quantities can be inferred. Therefore, three metrics of daily community production were determined from the observed diel variations in POC (Fig. 2), each incorporating different biogeochemical processes and providing a different perspective on them.

(1) Net community production (NCP; mg C m^{-2} d^{-1}) is defined here as the difference between POC estimates from

sunrise to the following sunrise. It is a measure of the net fixation or loss of particulate organic carbon over 24 h. (2) Daytime net community production (NCPd; mg C m^{-2} d^{-1}) was computed following Claustre et al. (2008; DΔPOC) as the daytime increase in POC (mg C m^{-2}) from sunrise to sunset. It accounts for the daytime carbon fixation and the daytime losses through respiration, grazing, and sinking. (3) An estimate of gross community production (GCP; mg C m^{-2} d^{-1}) was calculated as the difference between the daytime maximum POC and the theoretical sunset minimum POC, which solely takes into account community losses. Assuming equal community losses during daytime and nighttime, the theoretical sunset minimum is determined by applying the mean rate of POC decrease from the previous night ($0.5 < k < 1$) to the sunrise POC concentration. To account for potential differences in the timing of diel maxima of b_{bp} and c_p, the daytime maxima POC concentration is used rather than the sunset value.

In addition, shorter term variations of POC estimates are used to calculate a "real-time" net production (NCPh; mg C m^{-2} h^{-1}) representing the change in POC at 15 min intervals. To facilitate comparisons with primary production models, all community production data were depth-integrated to the depth of the euphotic zone following Gernez et al. (2011) assuming vertically homogenous ΔPOC. This assumption is supported by previous observations in open ocean waters (Siegel et al. 1989; Claustre et al. 2008) and is acceptable given the primary goal of comparing c_p- and b_{bp}-derived metrics. Likewise, it must also be noted that it was not possible to account for the effects of particle sinking on the proxies of community production.

Optically derived NCPd was compared with two standard chlorophyll-based models of primary production: the vertically generalized production model (PP_{VGPM}; Behrenfeld and Falkowski 1997) and a semianalytical model (PP_{M91}; Morel 1991; Antoine and Morel 1996). The calculation of PP_{VGPM} includes a measure of depth-integrated phytoplankton biomass, which is estimated from the product of euphotic depth and mean daily surface Chl *a* following Morel and Berthon (1989), as well as irradiance and a photoadaptive yield term, calculated from in situ BOUSSOLE sea surface temperature, and required to convert the estimated biomass into a photosynthetic rate. Mean daily Chl *a* concentration is determined from in situ BOUSSOLE pigment analyses (when available) combined with the SeaWiFs ocean color product as described in Antoine et al. (2008). For PP_{M91}, biomass is also estimated from this surface Chl *a*, but irradiance is spectrally dependent (and corrected for cloud cover), while physiological parameters are defined and quantified in Morel et al. (1996). Primary production and net community production may represent different processes, but comparisons allow for a greater understanding of seasonal phytoplankton dynamics around the BOUSSOLE site.

Results

Temporal variation of optical properties—Seasonal hydrographical and biological characteristics of the BOUSSOLE site are representative of midlatitude temperate trophic conditions and consistent with the Mediterranean "bloom" bioregion identified by D'Ortenzio and Ribera D'Alcalà (2009). From 2006 to 2011, the site was characterized by deep annual winter mixing with the mixed layer depth z_m regularly reaching beneath 100 m between January and March (Fig. 3A). Following an increase in PAR above 20 mol photons m^{-2} d^{-1}, z_m shoaled to between 5 and 50 m and stayed within this range until November. As z_m decreased, Chl *a* increased from below 0.3 mg m^{-3} to peak between 1 and 5 mg m^{-3} before returning to low concentrations. Thus, four main biogeochemical seasons could be defined based on z_m and Chl *a* characteristics following Gernez et al. (2011): winter mixing, spring bloom proliferation, bloom decline, and oligotrophy. Selection criteria and mean characteristics of these seasons are indicated in Table 1. While bloom, decline, and oligotrophy are defined based on Chl *a* concentrations, mixing is determined from z_m and thus may encompass both periods of low and brief periods of relatively high Chl *a*. Note that bloom here is defined as a period of increasing biomass and not by a period of increased biomass. By subsequently analyzing the diel variations of biogeochemical properties within each season, we are able to understand how these properties may be dependent upon seasonally varying physical conditions and seasonal changes in phytoplankton composition and concentration.

Mixing and oligotrophic seasons are by far the most prevalent, representing 22% and 57% of observations, respectively, while just 10% and 11% can be assigned to bloom and decline seasons (Table 1). Chl *a* concentrations were lowest during summer oligotrophy and were ca. 2.5 times higher during mixing. Both mean beam attenuation and particulate backscattering, however, were equal during mixing and oligotrophic seasons, suggesting a mismatch between Chl *a* and IOPs. Both c_p and b_{bp} were also quasi-equal during bloom proliferation and collapse. However, the relative increase between the mixing–oligotrophy values and those during the bloom–collapse was greater for c_p (2.4 fold) than for b_{bp} (1.8 fold), indicating that c_p showed greater seasonal variations than b_{bp}.

The c_p and b_{bp} time series also showed that although the temporal variability is, to the first order, driven by the seasonal cycle (Fig. 3B), mean daily c_p varied by an order of magnitude between 0.06 and 0.84 m^{-1} averaging 0.19 m^{-1} across the 6 yr time series. The lowest values were recorded during the exceptionally strong winter mixing of early 2006, while the highs were recorded during the 2006 and 2010 spring blooms. It is noteworthy, however, that the 2008 bloom (with the maximum observed Chl *a* concentrations) was not sampled for c_p or b_{bp}. Backscattering daily means also varied by an order of magnitude between 0.0004 and 0.0043 m^{-1} and were on average 140-fold lower than the beam attenuation daily means (Fig. 3C).

Diel cycles of c_p and b_{bp} vary both seasonally (Fig. 4) and interannually (Kheireddine and Antoine 2014) at BOUSSOLE. Two main differences are observed between the two IOPs that could affect calculations of community

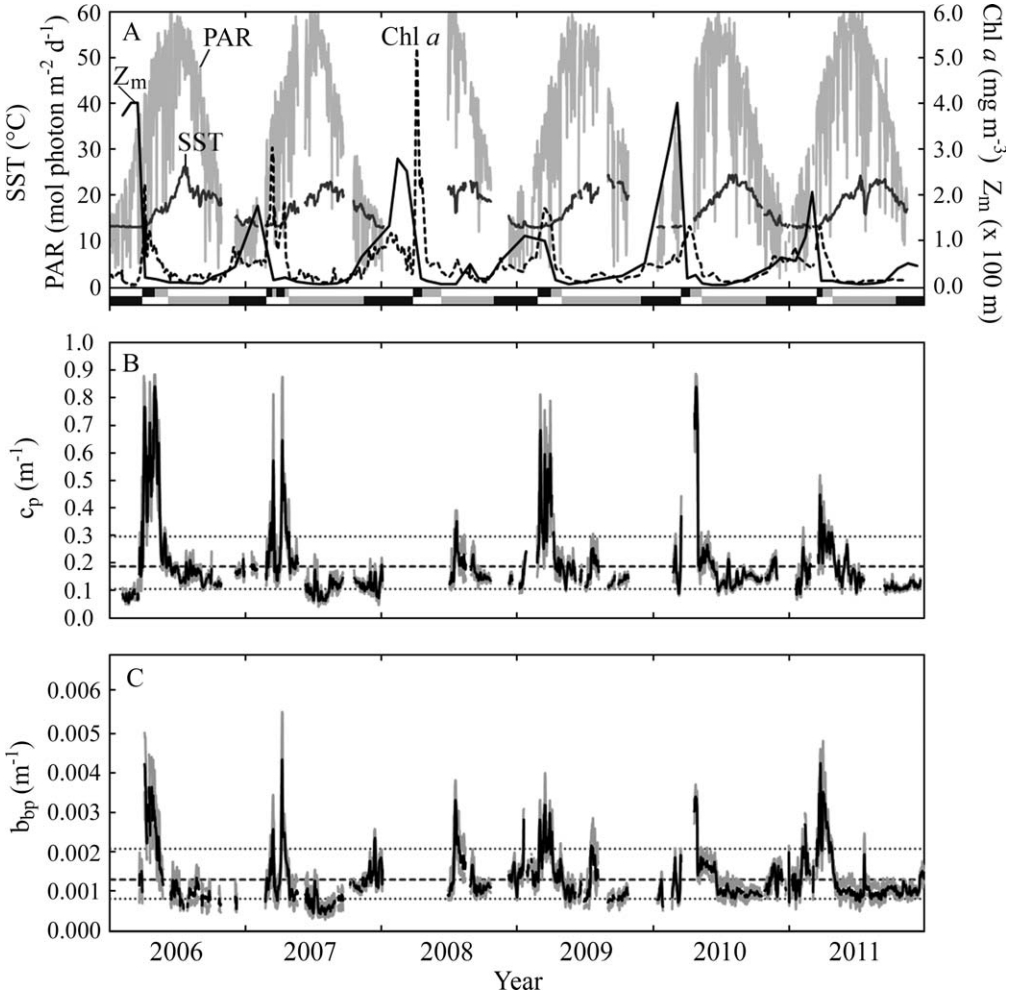

Fig. 3. Time series of (A) sea surface temperature (°C), Z_m (m), PAR (mol photons m^{-2} d^{-1}), and Chl *a* (mg m^{-3}); (B) daily mean (dark line) and minimum and maximum (light lines) c_p; (C) daily mean and minimum and maximum b_{bp}. Also shown are the seasons derived from Chl *a* and z_m (A, lower panel) upper dark, bloom; upper light, decline; lower dark, mixing; lower light, oligotrophy, and the median (dashed line) and (B, C) the 10% and 90% percentiles for c_p and b_{bp} across the time series.

production. Mean percentage variations from sunrise were significantly greater for c_p (Δc_p) than for b_{bp} (Δb_{bp}). The timing of the daily peak in b_{bp}, during decline, oligotrophy, and mixing seasons, was considerably earlier than that of c_p, and thus b_{bp} began decreasing longer before sunset than c_p. Combined, these processes resulted in smaller overall increases in b_{bp} from sunrise to sunset. During the vernal bloom, IOP values at sunset were on average 23.4% greater than at sunrise for c_p but just 11.9% greater for b_{bp}, while outside of the bloom b_{bp} values increased during daytime by 4.1–9.2%, whereas c_p increased by 13–14.4%. In addition to the two differences mentioned above, statistical analysis suggested a greater seasonal dependency of the diel variations of c_p than of b_{bp} (Tables 2 and 3). Significant differences were found between the sunrise–sunset increase in c_p during the bloom and that during the three other seasons, both in terms of percentage and absolute increase. Yet, despite significant differences between the sunrise–sunset percentage increase of b_{bp} during the bloom and that during collapse ($t = 2.17$, degrees of freedom (df) = 74,

Table 1. Selection criteria and mean biogeochemical characteristics of the four seasons differentiated for the BOUSSOLE time series (na indicating non applicable entries).

	No. of days		Criteria		Mean characteristics			
Season	c_p	b_{bp}	Chl *a* (mg m^{-3})	z_m (m)	z_m (m)	Chl *a* (mg m^{-3})	c_p (m^{-1})	b_{bp} (m^{-1})
Mixing	135	139	na	>80	174	0.51(±0.24)	0.16(±0.09)	0.0013(±0.0003)
Bloom	63	43	>0.6(↑)	na	34	1.39(±0.87)	0.38(±0.18)	0.0022(±0.0008)
Decline	74	60	>0.6(↓)	na	18	0.74(±0.48)	0.33(±0.19)	0.0020(±0.0007)
Oligotrophy	532	465	<0.6	na	15	0.20(±0.08)	0.14(±0.04)	0.0010(±0.0003)

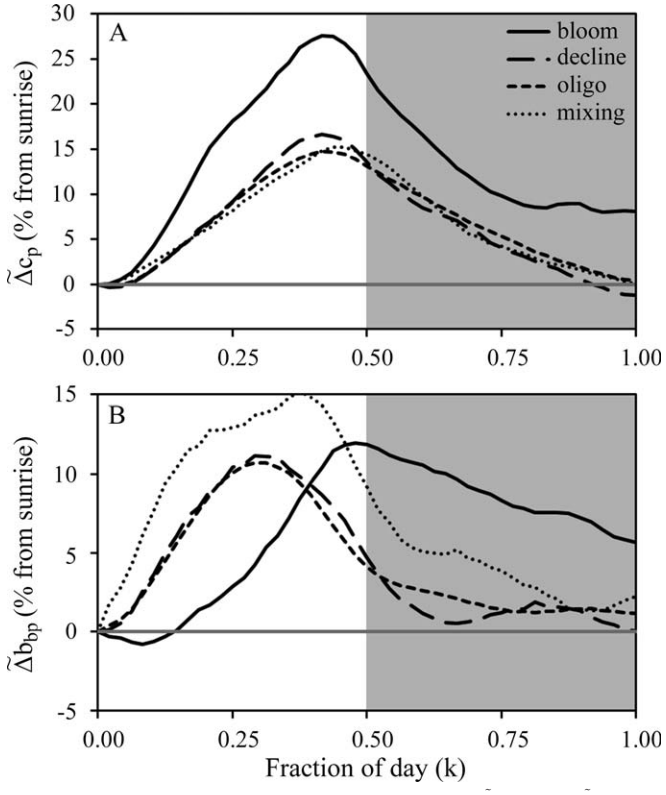

Fig. 4. Mean diel cycles, by season, of Δc_p and Δb_{bp} (% change from sunrise). The x-axis represents fractions of the normalized day (sunrise and sunset are 0 and 0.5, respectively). Oligo represents oligotrophy.

$p = 0.033$) and oligotrophy ($t = 2.71$, df = 44, $p = 0.010$), there were no significant seasonal variations of the absolute change in b_{bp} from sunrise to sunset for all pairs of seasons. Likewise, despite significant seasonal differences in the relative ($F = 4.97$, df = 3,800, $p = 0.002$) and absolute ($F = 6.46$, df = 3,800, $p < 0.001$) sunrise–sunrise variations in c_p, there was no significant seasonal variation in either relative ($F = 0.67$, df = 3,703, $p = 0.571$) or absolute ($F = 0.49$, df = 3,703, $p = 0.692$) sunrise–sunrise variation in b_{bp}.

Biogeochemical relationships—A linear relationship was observed between buoy c_p and Chl *a* (upper 10 m) across the time series (Fig. 5A). A couple of outliers with high c_p and low Chl *a* were observed when the percentage of microplankton (as determined from pigment composition) was relatively high (> 60%) suggesting that this relationship may be size class specific or taxa specific. For observations with lower percentages of microplankton, 82% of the variability in c_p was explained by in situ Chl *a*. The relationship between b_{bp} and Chl *a*, however, was best described by a power function (Fig. 5B) such that b_{bp} was relatively higher per unit chlorophyll for smaller pigment biomass. The variance explained by this relationship was, however, substantially lower. Yet again, the very highest contributions of microplankton were associated with relatively higher b_{bp}, though there were slightly fewer coincident b_{bp} and in situ Chl *a* measurements. The BOUSSOLE site undergoes strong seasonal changes in phytoplankton size structure with larger cells dominating during the spring bloom, nanoplankton dominating from May to June, nanoplankton and picoplankton dominating from August to December, and with mixed communities dominating during January–February (Fig. 5C). In the spring, when microplankton dominate, IOP-based estimates of phytoplankton biomass may therefore yield relatively higher measurements than Chl *a*–based estimates of phytoplankton biomass.

Overall, c_p and b_{bp} were strongly correlated ($r = 0.83$, $p < 0.001$) with a power-law relationship describing 68% of the variability between IOPs (Fig. 5D). However, clear differences were observed between oligotrophy–mixing and bloom–collapse. Although only encompassing a narrow and low range in values, a steeper slope in the relationship between b_{bp} and c_p was found during oligotrophy and mixing (ca. 0.0069 vs. 0.0045 during blooms). Thus, with increasing phytoplankton biomass, b_{bp} values increase more slowly than c_p.

Daytime net community production—In general, mean seasonal variations of c_p and b_{bp} are comparable both in terms of the timing of the spring maximum (mid-March to late-April) and in terms of relative amplitude of seasonal changes (Fig. 6A,B). Outside of the spring peak, substantially greater interannual and intraseasonal variations were observed for mean daily b_{bp} than for c_p. Daily means, however, did not necessarily reflect the amplitude of diel variations equally in both IOPs. Mean seasonal cycles of net community production, NCP, were similar for estimates based on c_p and b_{bp} with a mid-March annual peak (0.23 and 0.05 g C m^{-2} d^{-1}, respectively) and a mid-April trough (−0.23 and −0.14 g C m^{-2} d^{-1}, respectively; Fig. 6C,D). However, much greater variability was observed for NCP[c_p] than NCP[b_{bp}] particularly during March–April. The daytime net community production, NCPd, calculated from c_p also showed the greatest amplitude of variations during the spring bloom. During this time NCPd[c_p] varied between −5.9 and 7.2 g C m^{-2} d^{-1}, and the 10 d running mean peaked at 1.06 g C m^{-2} d^{-1} (Fig. 6E). Annual mean NCPd[c_p] was 0.63 g C m^{-2} d^{-1}, while the mean during March–April was 0.97 g C m^{-2} d^{-1}. In comparison, seasonal variations in NCPd[b_{bp}] were greatly reduced with no greater variability during the spring bloom than during the rest of the year (Fig. 6F). Annual mean NCPd[b_{bp}] was 0.11 g C m^{-2} d^{-1} and equal to the spring mean, which is almost an order of magnitude lower than NCPd[c_p] for the same period. The range of NCPd[b_{bp}] was also much lower, varying between −2.6 and 1.7 g C m^{-2} d^{-1}. Overall, the reduced seasonal variations in NCP[b_{bp}] and NCPd[b_{bp}] reflect the lack of seasonal dependency of the diel b_{bp} cycles. Similarly, b_{bp}-based gross community production estimates show a weaker springtime increase in mean and variance around the mean than for c_p (Fig. 6G,H). Highest annual 10 d mean GCP[c_p] attained was 2.02 g C m^{-2} d^{-1}, which occurred during late-March to early-April, toward the end of the peak in NCPd[c_p]. This period shows the greatest variability in GCP[c_p] and, to a lesser degree, in GCP[b_{bp}]. Overall, all three estimates of

Table 2. Seasonal dependence of the diel variations of both c_p and b_{bp} from sunrise to sunset and from one sunrise to the next calculated in terms of percentage change, absolute change, and net (or daytime net) community production. One-way ANOVA was performed to test for seasonal dependence, while *t*-tests were then used to determine the significant differences for each pair of seasons (B, bloom; D, decline; M, mixing; O, oligotrophy). Test statistics (*F* for ANOVA, *t* for *t*-tests), *p* and degrees of freedom (df) are shown and significant differences are marked in bold.

		Percentage change			Absolute change			NCP		
Fraction of day (k)	Test	*F* or *t*	*p*	df	*F* or *t*	*p*	df	*F* or *t*	*p*	Df
b_{bp} sunrise to sunset	ANOVA	**3.63**	**0.013**	**3703**	**10.55**	**0.000**	**3703**	**6.97**	**0.000**	**3703**
	B vs. D	**2.17**	**0.033**	**74**	1.86	0.068	50	0.82	0.416	58
	B vs. M	1.6	0.112	92	1.90	0.064	45	1.92	0.060	50
	B vs. O	**2.71**	**0.010**	**44**	2.02	0.050	42	0.69	0.493	43
	D vs. M	−0.59	0.557	183	−0.06	0.955	108	**2.06**	**0.042**	**117**
	D vs. O	0.28	0.779	69	0.20	0.843	62	−0.43	0.666	68
	M vs. O	0.99	0.321	155	0.41	0.681	158	**−3.96**	**0.000**	**183**
b_{bp} sunrise to sunrise	ANOVA	0.67	0.571	3703	0.49	0.692	3703	0.26	0.855	3703
	B vs. D	1.15	0.253	79	0.44	0.658	60	0.24	0.810	62
	B vs. M	0.43	0.669	109	0.34	0.736	45	0.26	0.794	49
	B vs. O	1.05	0.301	45	0.19	0.851	42	0.03	0.974	43
	D vs. M	−0.75	0.452	188	−0.28	0.779	83	0.01	0.993	105
	D vs. O	−0.46	0.647	69	−0.64	0.526	61	−0.47	0.642	66
	M vs. O	0.57	0.573	154	−0.72	0.470	166	−0.74	0.461	185
c_p sunrise to sunset	ANOVA	**10.4**	**0.000**	**3800**	**66.03**	**0.000**	**3800**	**19.3**	**0.000**	**3800**
	B vs. D	**2.66**	**0.009**	**88**	**3.03**	**0.003**	**79**	1.83	0.071	90
	B vs. M	**2.38**	**0.020**	**82**	**4.52**	**0.000**	**65**	**3.42**	**0.001**	**70**
	B vs. O	**3.03**	**0.004**	**64**	**4.90**	**0.000**	**62**	**3.19**	**0.002**	**63**
	D vs. M	−0.6	0.549	170	**3.24**	**0.002**	**103**	**2.72**	**0.008**	**115**
	D vs. O	0.25	0.804	86	**4.36**	**0.000**	**75**	**2.35**	**0.021**	**79**
	M vs. O	1.15	0.251	168	1.81	0.073	156	−1.17	0.243	180
c_p sunrise to sunrise	ANOVA	**4.97**	**0.002**	**3800**	**6.46**	**0.000**	**3800**	**3.99**	**0.008**	**3800**
	B vs. D	**2.04**	**0.044**	**97**	1.85	0.068	92	1.76	0.082	100
	B vs. M	1.73	0.087	78	1.34	0.186	64	1.33	0.188	68
	B vs. O	1.89	0.063	63	1.40	0.167	62	1.34	0.185	63
	D vs. M	−0.73	0.464	135	−1.39	0.169	83	−1.08	0.283	95
	D vs. O	−0.74	0.462	80	−1.32	0.190	74	−1.16	0.249	78
	M vs. O	0.17	0.861	167	0.36	0.717	177	−0.05	0.957	200

community production based on b_{bp}-derived POC show much less intraseasonal and interseasonal variation and lower amplitude than those derived from c_p.

Linear regressions between community production estimates based on either IOP further revealed the intraseasonal variability of these estimates (Fig. 7). Significant regressions were found for the relationships between NCP[c_p] and NCP[b_{bp}], NCPd[c_p] and NCPd[b_{bp}], and GCP[c_p] and GCP[b_{bp}] for pooled data as well as for individual seasons. Only for GCP estimates during the decline was there no significant relationship between estimates based on c_p and those based on b_{bp}. Overall, out of the three metrics tested, NCP showed the least amount of correlation between its estimates based on c_p and b_{bp} (Fig. 7A). Pooling all data, there was only 24.0% of shared variance between NCP[c_p] and NCP[b_{bp}], though the regression itself was significant (Table 4). The highest shared variance between estimates was obtained for NCPd (41.5%). For all three metrics, out of the four seasons, the highest adjusted R^2 values were obtained during the bloom (44.1–66.7%), while the lowest were found for the decline (1.5–18.3%). For the decline period the slope of the regression was also considerably lower than the other seasons (Fig. 7).

Table 3. Analogous statistics to Table 2 but for the seasonal dependence of gross community production determined using either b_{bp} or c_p.

	b_{bp}			c_p		
Test	*F* or *t*	*p*	df	*F* or *t*	*p*	Df
ANOVA	**3.52**	**0.015**	**3703**	**70.71**	**0.000**	**3800**
B vs. D	0.99	0.327	65	**3.18**	**0.002**	**77**
B vs. M	**2.18**	**0.033**	**53**	**5.93**	**0.000**	**67**
B vs. O	1.54	0.131	45	**5.51**	**0.000**	**63**
D vs. M	1.86	0.066	114	**6.50**	**0.000**	**125**
D vs. O	0.78	0.435	74	**5.88**	**0.000**	**83**
M vs. O	−1.85	0.066	219	**−2.28**	**0.024**	**188**

Having recognized the differences between the seasonal cycles observed for the community production metrics based on either IOP, in order to understand which, if any, conforms to our current understanding of seasonal biogeochemical dynamics at BOUSSOLE, this seasonality must be compared with more traditional biogeochemical estimates. NCPd[c_p] was compared with two chlorophyll-based models of ocean primary production. Two main differences exist between the techniques: they are forced by different biomass proxies and they represent different biological processes. Results from Fig. 5 have already indicated that the relationship between Chl *a* and c_p may

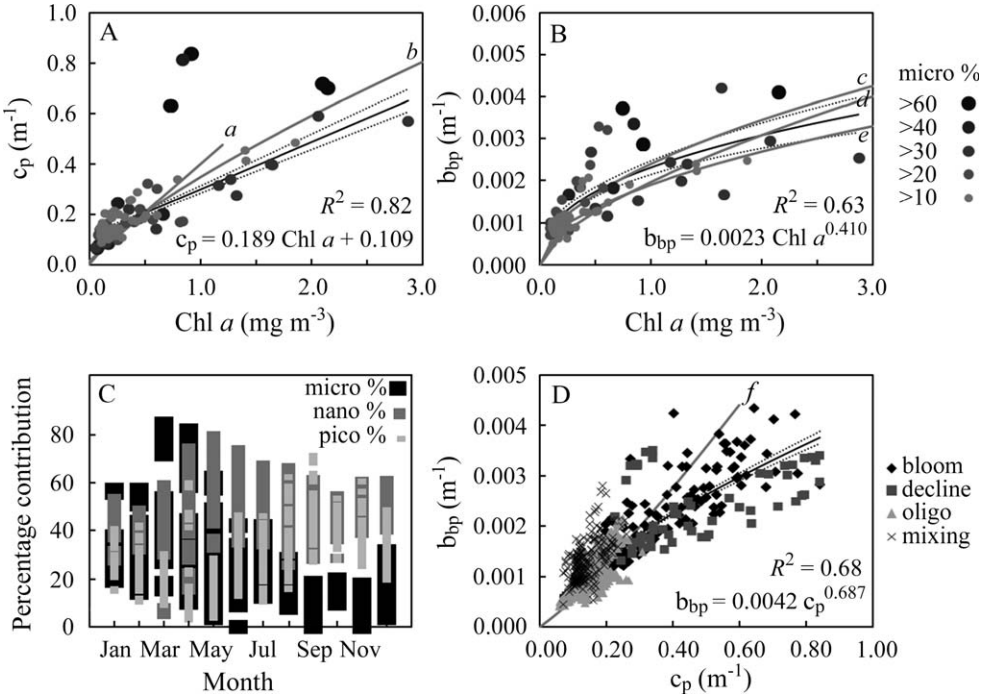

Fig. 5. Relationships between in situ Chl *a* and (A) c_p and (B) b_{bp}, (C) seasonal changes in phytoplankton size structure, and (D) the relationship between c_p and b_{bp}. (A, B) point size and color indicate the percentage of phytoplankton in the "micro" size class identified from accessory pigments. A linear regression (dark line) and associated 95% confidence interval is shown for (A) and performed on observations with < 60% microplankton. Power relationships for all observations are shown for (B) and (D). (C) points represent the percentage contribution of the three size classes for each pigment analysis across the time series, plotted by month. The relationships of (A) (*a*) Behrenfeld and Boss 2006 and (*b*) Loisel and Morel 1998; (B) (*c*) Huot et al. 2008, (*d*) Antoine et al. 2011, and (*e*) Stramska et al. 2003; (D) (*f*) Antoine et al. 2011 are indicated (gray lines).

not entirely be linear and may in fact vary with community composition and seasonally. Phenological differences between NCPd and estimates of primary production were therefore expected. The mean seasonal cycle of NCPd[c_p] was very similar, however, to that of primary production for the two models tested, both in terms of amplitude and phenology. For most of the year NCPd[c_p] was less than PP_{VGPM} and slightly greater than PP_{M91} (Fig. 8). Only during July–September is NCP[c_p] greater than both chlorophyll-based estimates of primary production.

Diel cycles of net community production—Although calculated from diel variations in IOPs, the estimates of NCPd shown above are daily totals dependent solely on sunrise, sunset, or maximal measurements and therefore can yield no information as to the diel cycles of productivity themselves. By considering finer-scale temporal variations in the IOPs, a higher resolution of the diel changes in POC is obtained, which in turn allows for examination of the diel characteristics of net community production.

Throughout the time series, c_p was observed to increase steadily from sunrise, peak about two-thirds of the temporal gap between midday and sunset, and then decrease steadily. During oligotrophy and mixing, there is no net change in c_p over 24 h, while c_p increases on average by 8.1% and decreases by 1.2% during bloom and decline seasons, respectively. During the decline of the bloom, the peak in c_p also occurred a few hours earlier. These seasonal differences in c_p have a predictable influence on NCPh diel cycles.

Diel cycles of NCPh[c_p] show relatively low intraseasonal variability, particularly during oligotrophic and mixing seasons (Fig. 9). A crude measurement of this variability is the 10–90 interpercentile range (IPR) relative to the amplitude of diel cycle. During the decline of the bloom, mixing, and oligotrophy, the ratio between the mean interpercentile range and the maximum diel range is equal to 1.47–1.50. This ratio is only slightly higher during bloom proliferation (1.74). During the bloom, maximum variability in NCPh[c_p] occurred prior to solar noon, with a 30% increase in IPR for k between 0.13 and 0.25 (ca. 0.025 g C m^{-2} h^{-1}), whereas during the decline the IPR was 25% greater for between 0.38 and 0.48. The IPR was relatively constant throughout the mixing and oligotrophic diel cycles. In accordance with previous observations, the greatest daytime NCPh[c_p] was recorded for the bloom proliferation (peak of mean cycle at 0.0069 g C m^{-2} h^{-1}) with intermediate values during the bloom decline (0.0028 g C m^{-2} h^{-1}) and greatly reduced values during mixing (0.0016 g C m^{-2} h^{-1}) and oligotrophy (0.0012 g C m^{-2} h^{-1}).

By comparison, NCPh[b_{bp}] showed much greater variability relative to the range of mean diel variations

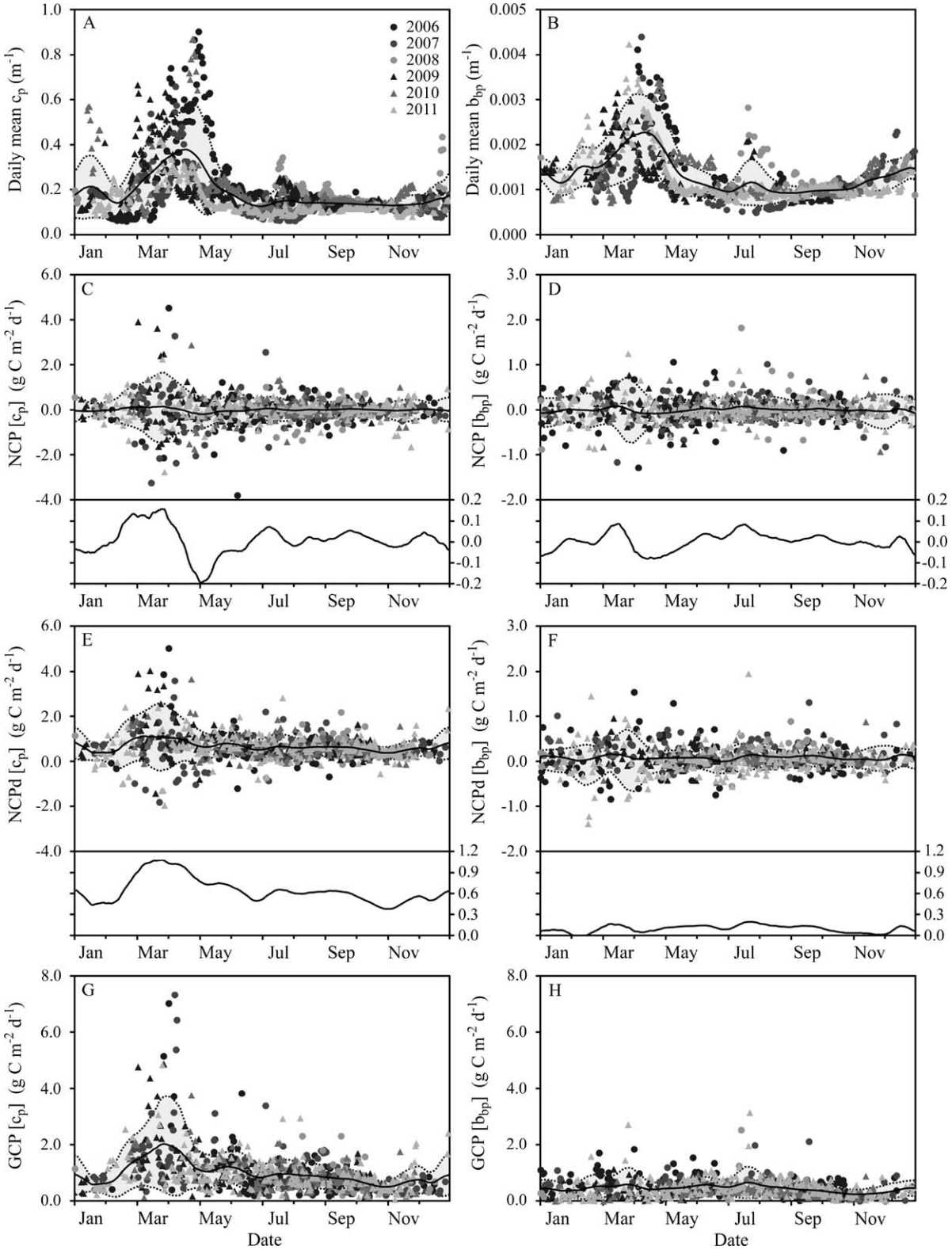

Fig. 6. Seasonality of the daily mean of IOPs (A) c_p and (B) b_{bp}, and three estimates of community production, NCP, NCPd, and GCP calculated from temporal evolution of c_p (C, E, and G, respectively) and b_{bp} (D, F, and H). Data are shown by year with a 10 d running mean (solid line) and standard deviations (dotted line) across the whole time series. (D, F) running means are also shown beneath each graph with an expanded y-axis for clarity.

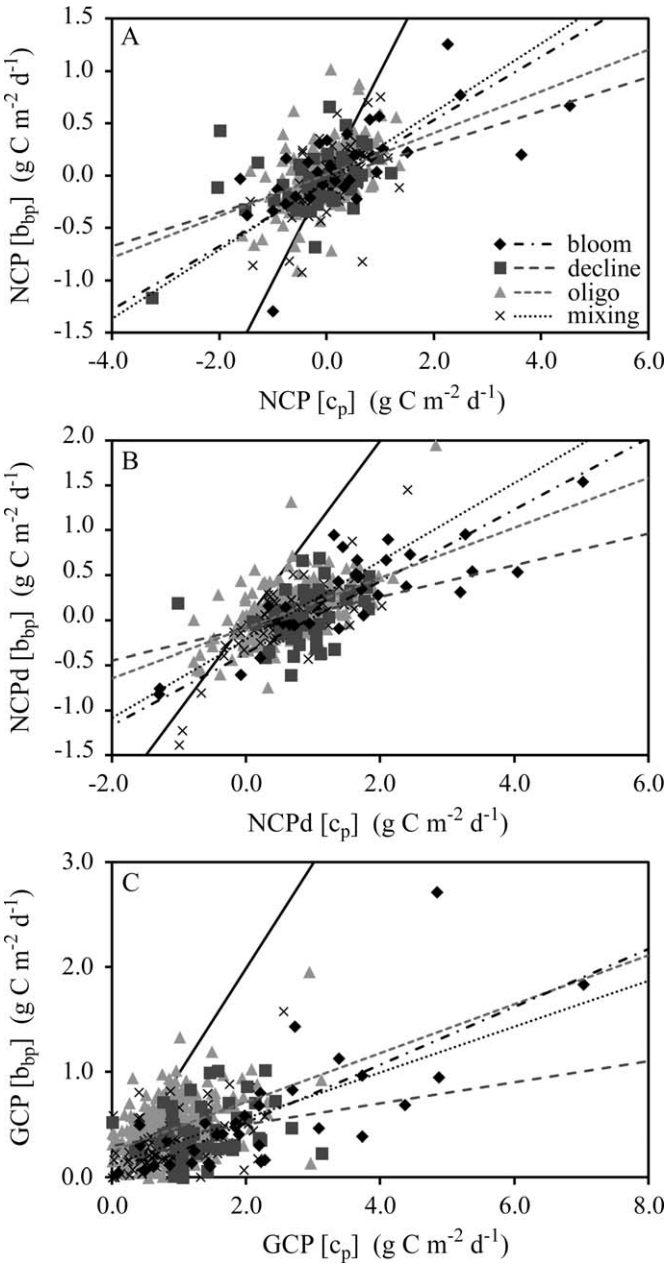

Fig. 7. Relationships between (A) NCP, (B) NCPd, and (C) GCP calculated from c_p and b_{bp}. Data are shown by season with a linear regression plotted for each season and the 1 : 1 line is shown (solid line).

(Fig. 10). Indeed, for all four seasons the ratio between IPR and diel range was greater than 3.1 (double that of NCPh[c_p]) and reached 5.9 during mixing when the mean amplitude of diel variations was particularly low. This was primarily due to the low amplitude of mean diel variations, which was 2.3 (for oligotrophy) to 5.5 (for the bloom) times lower than for NCPh[c_p]. Accordingly, maxima of the four mean diel cycles of NCPh[b_{bp}] were of just 0.0013 (bloom), 0.0008 (decline), 0.0004 (mixing), and 0.0005 (oligotrophy) g C m^{-2} h^{-1}. For all four seasons, IPR was much greater during daytime in general, representing a 30% increase over nighttime IPR for bloom, decline, and mixing seasons and a 67% increase during oligotrophy.

Diel cycles of NCPh[c_p] show remarkable consistency in timing between seasons (Fig. 11A). The daytime peak occurred a little before solar noon (ca. k = 0.20) with little variation for k between 0.10 and 0.30. Pairwise Kuiper's *V*-tests (for cyclic data; Kuiper 1960) between seasons revealed no significant seasonal differences of the timing of the diel maximum ($V < 0.160$, $0.105 < p < 0.719$). The maximal rate of decrease of NCPh[c_p] during all seasons was observed after k = 0.40, while the diel minima were consistently recorded just after sunset, following which NCPh[c_p] increased steadily during hours of darkness. Conversely, strong interseasonal differences in the NCPh[b_{bp}] diel cycles were evident (Fig. 11B). Statistical analysis reveals significant differences in the timing of the diel NCPh[b_{bp}] maxima between the bloom seasons and those of mixing ($V = 0.347$, $p = 0.019$) and oligotrophy ($V = 0.449$, $p < 0.001$) as well as between oligotrophy and mixing ($V = 0.313$, $p < 0.001$). The peak during mixing occurred several hours before that of oligotrophy, itself occurring hours before the afternoon peak during blooms. These results indicate that even though there may not be seasonal differences in the total daytime net community production derived from b_{bp}, there may be significant differences in the timing of the diel production cycles.

Discussion

Time scales of particulate variability at BOUSSOLE—Across the 6 yr time series, the principal mode of variation of both c_p and b_{bp} was seasonal in accordance with annually recurrent vernal phytoplankton blooms with occasional other increases such as during autumn 2009. Throughout the rest of the year, however, diel variations are often greater than variations in the daily mean from one day to the next. During analysis, data were filtered for strong advection events on the basis of salinity and temperature time series and sensor depth. Therefore the assumption is made that the diel cycles in c_p and b_{bp} obtained here are not significantly affected by diurnal changes in the mixed layer depth and essentially result from biological activity. This hypothesis is supported by Gernez et al. (2011), who observed only ca. 2% differences in mean c_p between estimates of fixed and variable mixed layer depth.

The diurnal increase of c_p results from the accumulation of intracellular carbon associated with photosynthetic processes, which is coupled with changes in phytoplankton properties, particularly an increase in refractive index and size (Siegel et al. 1989; Stramski and Reynolds 1993; Claustre et al. 2002). Conversely, losses of particulate matter occur throughout the day due to phytoplankton respiration and excretion, cell division, and cell mortality through grazing activity and viral lyses (Cullen et al. 1992; Stramski and Reynolds 1993). In accordance with replete light and nutrient conditions, the amplitude of these cycles is highest during the bloom when phytoplankton, which show the greatest tendency towards diel variation, contribute the greatest proportion of c_p variability (Fig. 4A). The

Table 4. Linear regression statistics for community production (CP) metrics derived from b_{bp} vs. c_p. All slope and intercept values were statistically significant (at 5%) except for those denoted with an asterisk.

		$CP[b_{bp}] = a \times CP[c_p] + b$		Regression statistics		
CP	Season	*a*	*B*	*F*	*p*	R^2 (%)
NCP	all	0.2413(±0.0184)	−0.0034(±0.0107)*	$F_{1,539}=171.9$	$p<0.001$	24.0
	M	0.3289(±0.0593)	−0.0448(±0.0286)*	$F_{1,79}=30.7$	$p<0.001$	27.1
	B	0.3015(±0.0585)	−0.0726(±0.0849)*	$F_{1,31}=26.6$	$p<0.001$	44.4
	D	0.1616(±0.0472)	−0.0288(±0.0384)*	$F_{1,47}=11.7$	$p=0.001$	18.3
	O	0.1986(±0.0270)	0.0105(±0.0109)*	$F_{1,376}=53.9$	$p<0.001$	12.3
NCPd	all	0.3188(±0.0166)	−0.1338(±0.0153)	$F_{1,539}=369.0$	$p<0.001$	41.5
	M	0.4347(±0.0433)	−0.2150(±0.0370)	$F_{1,79}=100.7$	$p<0.001$	55.5
	B	0.3996(±0.0495)	−0.3668(±0.0992)	$F_{1,31}=65.2$	$p<0.001$	66.7
	D	0.1757(±0.0782)	−0.0944(±0.0786)*	$F_{1,47}=5.05$	$p=0.029$	7.8
	O	0.2786(±0.0232)	−0.0851(±0.0176)	$F_{1,376}=144.8$	$p<0.001$	27.6
GCP	all	0.2061(±0.0148)	0.2242(±0.0179)	$F_{1,539}=194.8$	$p<0.001$	26.4
	M	0.2184(±0.0407)	0.1239(±0.0419)	$F_{1,79}=28.8$	$p<0.001$	25.8
	B	0.2754(±0.0436)	−0.0323(±0.1162)*	$F_{1,31}=39.9$	$p<0.001$	54.8
	D	0.1005(±0.0582)*	0.3002(±0.0871)	$F_{1,47}=2.99$	$p=0.091$*	4.0
	O	0.2365(±0.0242)	0.2353(±0.0237)	$F_{1,376}=95.3$	$p<0.001$	20.0

amplitude and timing of the backscattering also showed a marked difference during the annual spring bloom, though the increase in amplitude during the bloom was only slight compared with that of c_p.

Both c_p and b_{bp} co-vary with the concentration of particles, which in regions of low concentrations and low scattering from inorganic matter have been used as proxies for POC (Gardner et al. 2006; Stramski et al. 2008; Bishop 2009). However, c_p and b_{bp} differ with respect to the size of particles they are most influenced by. While Mie scattering theory suggests b_{bp} is dominated by submicron particles (Vaillancourt et al. 2004) and phytoplankton are not thought to be a major contributor to b_{bp} (Stramski and Kiefer 1991), laboratory studies have shown a much larger effect of phytoplankton on b_{bp}, with up to 70% of b_{bp} variability associated with changes in phytoplankton abundance (Dall'Olmo et al. 2009; Martinez-Vicente et al. 2012). Loisel et al (2007) showed that in Case 1 waters, it was the slope of the particle size distribution (and not the refractive index) that was the predominant factor controlling the temporal variability in b_{bp}, which has also been observed at BOUSSOLE (Kheireddine and Antoine 2014).

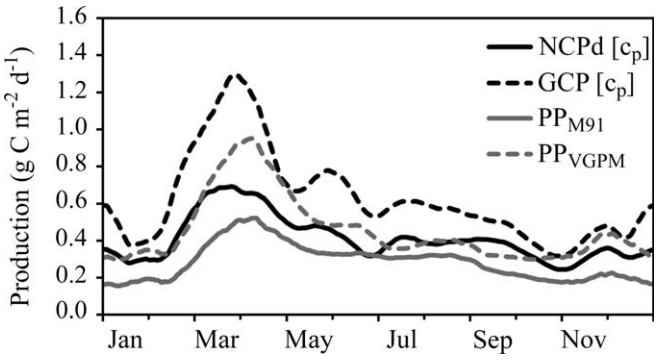

Fig. 8. Mean seasonal cycles of NCPd calculated from c_p and primary production calculated according to two chlorophyll-based models: the semianalytical model of Morel (1991; PP_{M91}) and the vertically generalized model of Behrenfeld and Falkowski (1997; PP_{VGPM}).

It is likely that the first driver of diel particle growth is phytoplankton, yet small heterotrophs (0.1–10 μm in size) have been shown to exhibit diel cycles of activity (Mével et al. 2008) and contribute significantly to the c_p diel cycle (Oubelkheir and Sciandra 2008). Heterotrophic bacteria, in particular, might explain a third of the spatial variability of c_p in oceanic regions (Montes-Hugo et al. 2009). Separating the diel effects of phytoplankton and heterotrophs is further complicated by the tight synchronicity between the photosynthetic extracellular release of organic material and bacterial consumption as observed for instance in the Mediterranean Sea (Gasol et al. 1998; Mével et al. 2008) and the North Pacific Ocean (Church et al. 2004). Insufficient data were available here to fully explain the causes of these seasonal variations and differences between both optical properties.

Differences between biogeochemical proxies for phytoplankton carbon—Backscattering showed a weak power-law relationship with Chl *a*, consistent with observations in the north polar Atlantic (Stramska et al. 2003), the south Pacific gyre (Huot et al. 2008), and early BOUSSOLE observations (Antoine et al. 2011). Beam attenuation varied linearly with Chl *a* in agreement with observations by Behrenfeld and Boss (2006). Under high concentrations of microplankton, c_p and, to a lesser extent, b_{bp} were greater than could be predicted by the total relationship with Chl *a*. Although this represents only a small number of observations, this could be indicative of higher carbon to chlorophyll ratios for the larger size classes as well as the larger cells not being well represented by b_{bp}. Aside from size structure considerations of relating each IOP to phytoplankton carbon, variability of the C : Chl *a* ratio has been attributed to physiological changes such as photoacclimation (Behrenfeld et al. 2005) as well as community composition (Whitmire et al. 2010). Owing to these and other processes (e.g., package effect), the

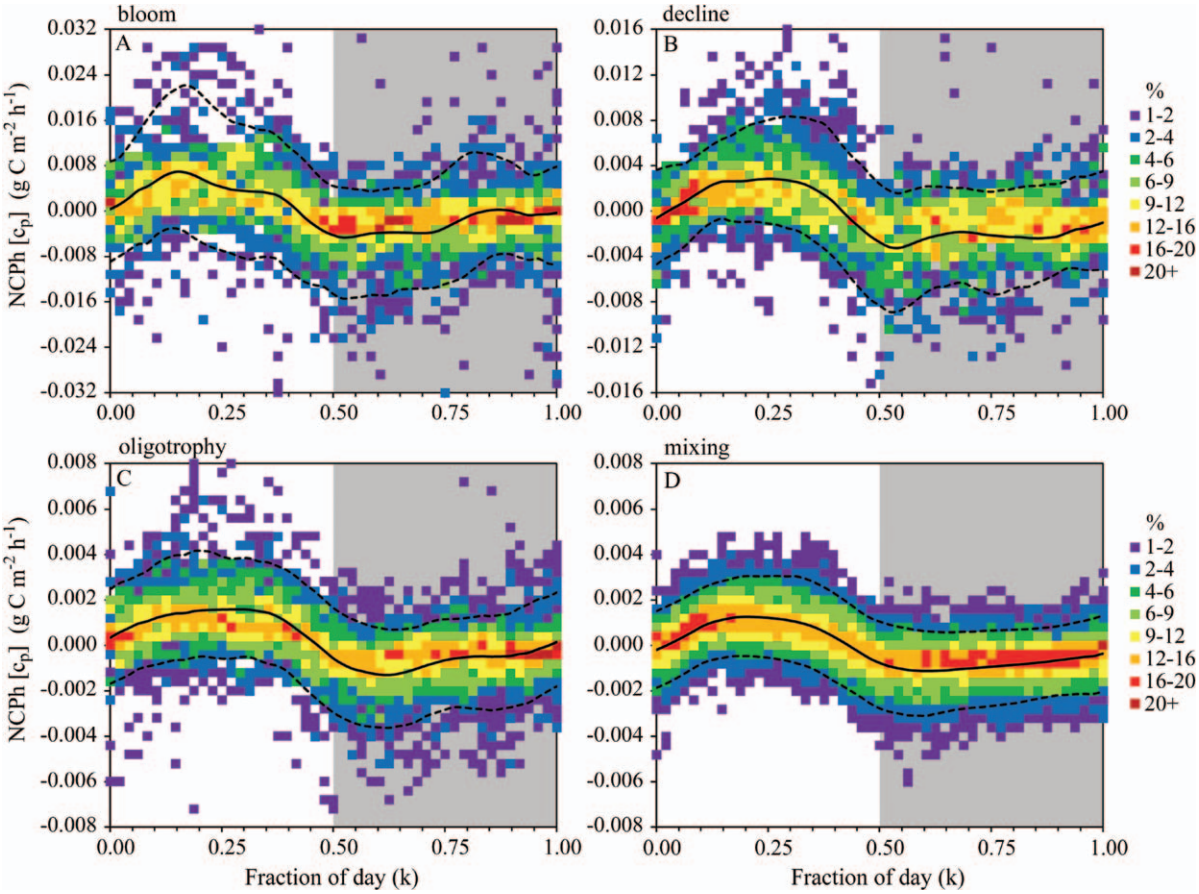

Fig. 9. Daily profiles of NCPh calculated from c_p for the (A) bloom, (B) decline, (C) oligotrophy, and (D) mixing seasons. The x-axis represents fractions of the normalized day (sunrise and sunset are 0 and 0.5, respectively). Time series running means (solid line) and 10 and 90 percentiles (dashed lines) are shown. Color indicates for each k (in 1 : 48 $\approx$ 30 min bins) the percentage of NCPh data within each (A) 0.0016, (B) 0.0008, and (C, D) 0.0004 g C m^{-2} h^{-1} bins.

historical use of Chl *a* as a proxy of phytoplankton biomass or production has been called into question (Marra et al. 2007). These results highlight that all three parameters differ in the processes and particles they are influenced by, and any modeled relationships between them must take into account the scales of variation of such processes.

Daily production from POC—Knowledge of the b_{bp} vs. c_p relationship in the open ocean is limited because of the few, albeit growing, number of concurrent measurements. Comparable diel and seasonal changes in c_p and b_{bp} would allow them to be used interchangeably to derive information on the particulate pool and thus to estimate net community production of the ecosystem (Siegel et al. 1989; Claustre et al. 2008). Reasonably good correlations have previously been observed between c_p and b_{bp} (Dall'Olmo et al. 2009; Westberry et al. 2010; Antoine et al. 2011). Here also, we found relatively good correlations between c_p and b_{bp} daily means (Fig. 5C) and similar seasonal variability (Fig. 6A,B). Such results lend credence to the possibility of deriving c_p from remote sensing observations (Stramska and Stramski 2005) such as is already the case for b_{bp}. Yet, at BOUSSOLE, c_p and b_{bp} have been shown to display significant differences in the timing and amplitude of their diel cycles (Fig. 4). Outside bloom proliferation, maximal b_{bp} values occur earlier than those of c_p, while the amplitude of the diel cycle is substantially lower for b_{bp}. Furthermore, the relationship between c_p and b_{bp} appears dependent on the trophic status with a lower slope during bloom collapse than bloom proliferation (Fig. 5C). For these reasons, we found clear differences between estimates of community production based on either IOP.

At a first glance, the significant regressions (Table 4) observed for most production metrics (for both pooled data and individual seasons) suggest b_{bp} could be used to obtain estimates of net, daytime net, and gross community production similar to those calculated from diel variation in c_p. However, several observations suggest b_{bp}-derived community production metrics differ substantially from those based on c_p: (1) the weak slope of the regressions (Fig. 7), (2) the weak shared variance between daily production metrics (Table 4), and (3) the differing mean seasonal cycles (Fig. 6C–H) indicate that the metrics used here vary between both IOPs. Furthermore the agreement between c_p- and b_{bp}-derived metrics was largely seasonally dependent. For both CP[c_p] and CP[b_{bp}] greatest variability was found during the spring bloom proliferation and the greatest shared variance was found during this period

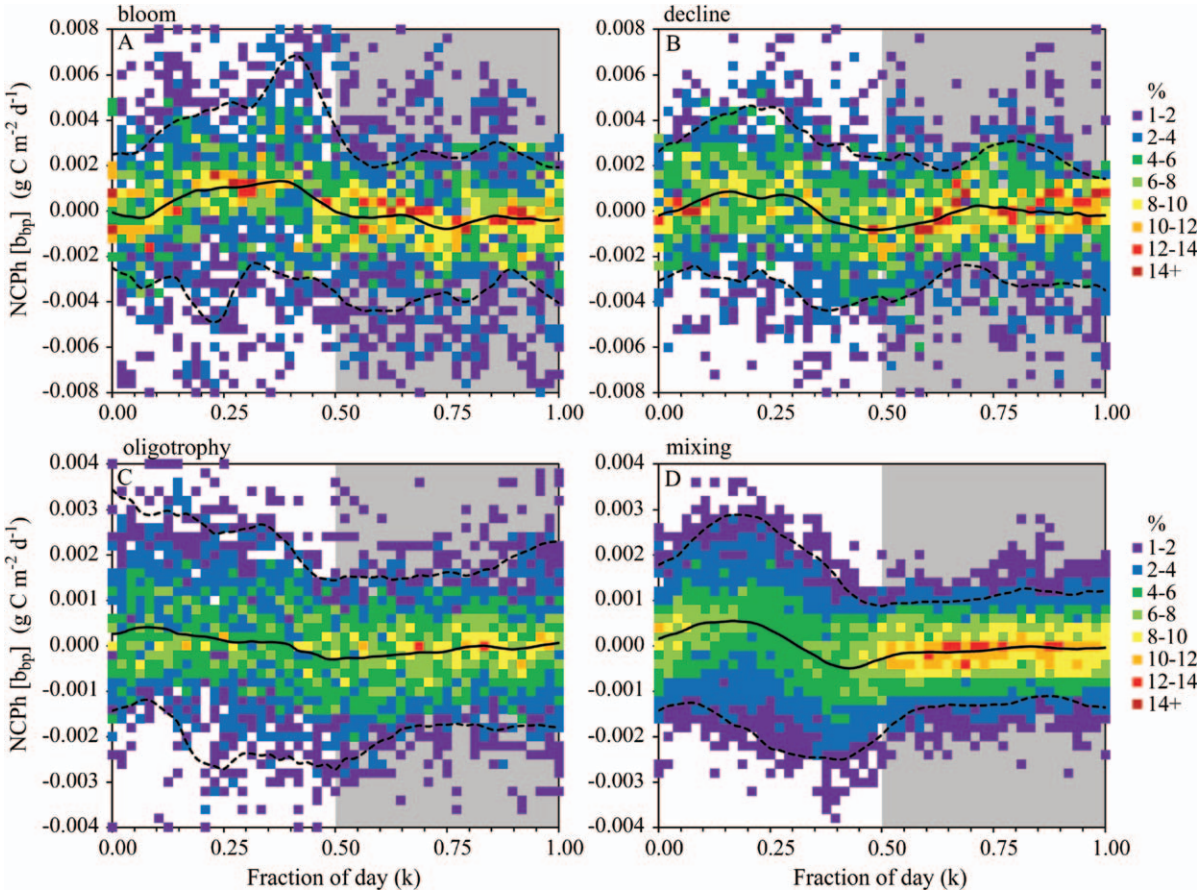

Fig. 10. Same as Fig. 9 for NCPh calculated from b_{bp}. NCPh bins are of (A, B) 0.0004 and (C, D) 0.0002 g C m^{-2} h^{-1}.

(Table 4), yet this was barely reflected in the mean spring seasonality of b_{bp}-derived daily production metrics (Fig. 6D, F,H). This was likely due to the poor agreement during the other seasons (except perhaps for NCPd during winter mixing) and, for NCPd, the insignificant differences in seasonal means.

Community production derived from either IOP also differed in terms of the diel cycles of NCPh and the timing of the diel maxima (Figs. 9, 10). Far greater intraseasonal variability (relative to the mean diel amplitude) was found for NCPh[b_{bp}], suggesting the particles contributing to backscattering show considerably lower diel variation. It is unclear to what extent this increased variability is due to the measurement noise inherent to backscattering measurement in clear waters. In addition, peak NCPh[b_{bp}] varied seasonally, trailing NCPh[c_p] during the bloom and leading it during mixing. It is likely that three main characteristics of b_{bp} diel variability contribute to the poor estimations of b_{bp}-derived estimates of community production: (1) the weak amplitude of b_{bp} cycles and the weak relative increase in amplitude during the bloom seasons, (2) the observed temporal lag between c_p and b_{bp} cycles, and (3) the seasonal dependency of this lag. These characteristics could result from the different size (and thus community) composition driving the variability in beam attenuation and backscattering. Also, b_{bp} excludes the absorption that is included in c_p. With recent studies confirming the key role of absorption in determining primary production (Barnes et al. 2014), these differences render b_{bp} a poor diagnostic of total community production at BOUSSOLE at the diel time scale.

Mean seasonal variations of NCPd[c_p] were comparable with net primary production (NPP) estimates from the chlorophyll-based models of Behrenfeld and Falkowski (1997; PP_{VGPM}) and Morel (1991; PP_{M91}). NPP and NCP differ in the processes they represent. Although NCP includes heterotrophic growth and losses, NPP concerns only autotrophic organisms. As such, it would be expected for NCPd to be lower than NPP estimates, although because NCPd more accurately reflects only the daytime changes in the carbon pool, it is higher than total NCP, which takes into account nighttime losses. The variation of primary production is consistent with seasonal cycles reported by Marty and Chiaverini (2002) between 1993 and 1999. All three estimates agreed with the late March–early April timing of the peak in production, the rate of increase during the prior months, and the rate of decrease in the subsequent months. This is somewhat surprising due to the observed differences between Chl *a* (forcing the PP_{VGPM} and PP_{M91}) and c_p, particularly during periods of high percentage of microplankton such as during March–April. The amplitude of NCPd[c_p] was found in between that of the PP_{VGPM} and PP_{M91}, with only a secondary peak of NCPd[c_p] in September superior to PP_{VGPM}.

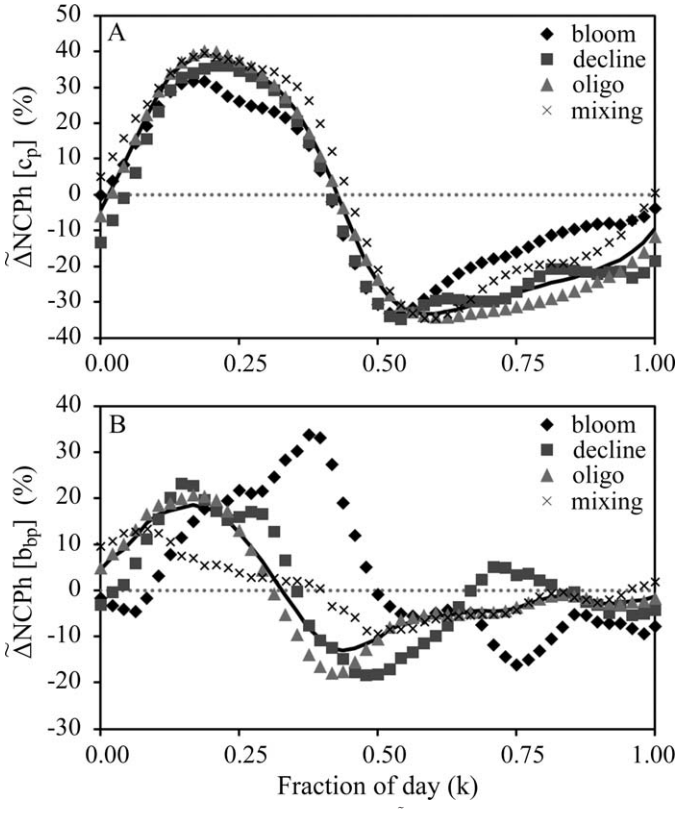

Fig. 11. Mean diel cycles of ΔNCPh (% of the daily maximum) for each season derived from (A) c_p and (B) b_{bp}. Total time series mean is also shown (solid line).

The use of optical properties to determine phytoplankton carbon is further complicated by the reported variability in the relationships between POC and attenuation or backscattering (Gardner et al. 2006; Cetinic et al. 2012). Regional differences in the slope of the c_p–POC (Fennel and Boss 2003) and b_{bp}–POC relationship (Allison et al. 2010) imply universal relationships between c_p or b_{bp} and particulate or phytoplankton carbon may not exist, though filtration methodological differences and varying pore sizes make comparisons difficult (Bishop et al. 2012). While it is possible that the shallow slope of the relation between CP[b_{bp}] and CP[c_p] metrics (Table 4) could be due in part to an erroneous parameterization of the relationship between b_{bp} (or c_p) and POC, it is unlikely that the b_{bp} : POC ratio be overestimated by more than fivefold. Furthermore, the slope of the relationship between POC and c_p is thought to vary with phytoplankton community composition (Claustre et al. 2002; Cetinic et al. 2012), and even diel variations have been shown for cultured species (Claustre et al. 2002). In situ POC measurements would be required to accurately assess the effects of such variations upon IOP-based estimates of seasonal or diel production, and although such measurements are presently being undertaken at the BOUSSOLE site, none were available for 2006–2011.

Diel cycles of community production—The shape and timing of the diel cycles of NCPh[c_p] agrees with earlier observations (Gernez et al. 2011) of the diel cycles in *r* (the rate of change of c_p) but differs from previous observations and models (Siegel et al. 1989; Cullen et al. 1992; Marra 1997). Unlike the later studies on the rate of change of c_p, the amplitude of NCPh was not synchronous with PAR. Maximal production occurred before noon in all seasons, and production became negative before sunset. This is consistent with laboratory observations of c_p (Stramski and Reynolds 1993) and phytoplankton photosynthesis (Harding et al. 1981; Prezelin 1992). NCPh[c_p] was in fact lowest around sunset, with a characteristic dip in production over a 1–2 h period. This could be related to phasing of phytoplankton cellular division or diel variations in grazing pressure. Phasing of cell division is linked to growth rates and occurs when the average population growth rate is less than or equal to one doubling per day during a defined interval relative to the light and dark cycle (Vaulot and Chisholm 1987), although this is thought to vary between species (Brunet et al. 2008). Diel activity of zooplankton grazing has also been observed, although grazing pressure is more or less constant during the hours of darkness (Welschmeyer et al. 1984). Following sunset, NCPh[c_p] remains negative and shows the least amount of intraseasonal variability during nighttime.

The BOUSSOLE time series has permitted the characterization of IOP variations with high temporal resolution across several annual cycles. This study has demonstrated the use of high-resolution beam attenuation measurements for investigating carbon accumulation of the particulate assemblage. In these Case 1 waters, the relative lack of inorganic particles has facilitated the interpretation of these cycles as being a result of organic growth, respiration, division, and consumption. Yet insufficient concomitant measurements of the biological composition and size were available to elucidate exactly what part of the particulate assemblage was being observed here—and thus which components of the biota were driving either c_p or b_{bp} variations. Furthermore, this study was restricted to the predominantly oligotrophic BOUSSOLE waters. Areas of basin-scale blooms or substantial upwelling, for instance, may have sufficient diel changes in b_{bp} to allow for b_{bp}-based determinations of community production. It is clear that further research is necessary if particulate backscattering is to be used to infer short-term temporal variations in organic carbon. With recent advances in automated platforms and sensors measuring phytoplankton composition (Sosik and Olson 2007) or particle size distribution (Reynolds et al. 2010), our ability to understand circadian rhythms in oceanic ecosystems is only improving.

Acknowledgments

We are grateful to the Bouée pour l'Acquisition de Séries Optiques à Long Terme (BOUSSOLE) technical staff for their work in performing laboratory analyses, buoy deployments, and monthly cruises, and to the captains and crews of R/Vs *Tethys-II*, *Antea*, and *Europe*. In particular, thanks go to Emilie Diamond and Melek Golbol for the monthly cruises, Joséphine Ras and Mustapha Ouhssain for the high-performance liquid chromatography pigment analyses, Vincenzo Vellucci for the optical data calibration, and Bernard Gentili for the photosynthetically active radiation processing. This research contributed to the Bio-Optics and Carbon Experiment (BIOCAREX) project, which is funded

by the Agence Nationale de la Recherche (ANR, Paris) and to the BOUSSOLE project. Financial, technical, and logistical support to the BOUSSOLE project was provided by the Centre National d'Etudes Spatiales (CNES), the Centre National de la Recherche Scientifique (CNRS), the European Space Agency (ESA), the Institut National des Sciences de l'Univers (INSU), the National Aeronautics and Space Administration (NASA), the Observatoire Océanologique de Villefranche sur Mer (OOV), and the Université Pierre et Marie Curie (UPMC).

References

Allison, D. B., D. Stramski, and B. G. Mitchell. 2010. Empirical ocean color algorithms for estimating particulate organic carbon in the Southern Ocean. J. Geophys. Res. **115:** C10044, doi:10.1029/2009JC006040

Antoine, D., P. Guevel, J. F. Deste, G. Becu, F. Louis, A. J. Scott, and P. Bardey. 2008. The "BOUSSOLE" buoy—a new transparent-to-swell taut mooring dedicated to marine optics: Design, tests, and performance at sea. J. Atmos. Ocean. Technol. **25:** 968–989, doi:10.1175/2007jetcho563.1

———, and A. Morel. 1996. Oceanic primary production .1. Adaptation of a spectral light-photosynthesis model in view of application to satellite chlorophyll observations. Glob. Biogeochem. Cycles **10:** 43–55, doi:10.1029/95gb02831

———, D. A. Siegel, T. Kostadinov, S. Maritorena, N. B. Nelson, B. Gentili, V. Vellucci, and N. Guillocheau. 2011. Variability in optical particle backscattering in contrasting bio-optical oceanic regimes. Limnol. Oceanogr. **56:** 955–973, doi:10.4319/lo.2011.56.3.0955

———, and others. 2006. BOUSSOLE: A joint CNRS-INSU, ESA, CNES and NASA ocean color calibration and validation activity. NASA Technical memorandum.

Barnes, M. K., G. H. Tilstone, T. J. Smyth, D. J. Suggett, R. Astoreca, C. Lancelot, and J. C. Kromkamp. 2014. Absorption-based algorithm of primary production for total and size-fractionated phytoplankton in coastal waters. Mar. Ecol. Prog. Ser. **504:** 73–89, doi:10.3354/meps10751

Behrenfeld, M. J., and E. Boss. 2006. Beam attenuation and chlorophyll concentration as alternative optical indices of phytoplankton biomass. J. Mar. Res. **64:** 431–451, doi:10.1357/002224006778189563

———, ———, D. A. Siegel, and D. M. Shea. 2005. Carbon-based ocean productivity and phytoplankton physiology from space. Glob. Biogeochem. Cycles **19:** 14, doi:10.1029/2004GB002299

———, and P. G. Falkowski. 1997. Photosynthetic rates derived from satellite-based chlorophyll concentration. Limnol. Oceanogr. **42:** 1–20, doi:10.4319/lo.1997.42.1.0001

Bishop, J. K. B. 2009. Autonomous observations of the ocean biological carbon pump. Oceanography **22:** 128–193, doi:10.5670/oceanog.2009.48

———, P. J. Lam, and T. J. Wood. 2012. Getting good particles: Accurate sampling by large volume in-situ filtration. Limnol. Oceanogr.: Methods **10:** 681–710, doi:10.4319/lom.2012.10.681

Boss, E., W. S. Pegau, M. Lee, M. Twardowski, E. Shybanov, G. Korotaev, and F. Baratange. 2004. Particulate backscattering ratio at LEO 15 and its use to study particle composition and distribution. J. Geophys. Res. Oceans **109:** 10, doi:10.1029/2002jc001514

Bricaud, A., A. Morel, and L. Prieur. 1981. Absorption by dissolved organic matter of the sea (yellow substance) in the UV and visible domains. Limnol. Oceanogr. **26:** 43–53, doi:10.4319/lo.1981.26.1.0043

Brunet, C., R. Casotti, and V. Vantrepotte. 2008. Phytoplankton diel and vertical variability in photobiological responses at a coastal station in the Mediterranean Sea. J. Plankton Res. **30:** 645–654, doi:10.1093/plankt/fbn028

Cetinic, I., M. J. Perry, N. T. Briggs, E. Kallin, E. A. D'Asaro, and C. M. Lee. 2012. Particulate organic carbon and inherent optical properties during 2008 North Atlantic Bloom Experiment. J. Geophys. Res. Oceans **117:** 18, doi:10.1029/2011jc007771

Church, M. J., H. W. Ducklow, and D. A. Karl. 2004. Light dependence of H-3 leucine incorporation in the oligotrophic North Pacific ocean. Appl. Environ. Microbiol. **70:** 4079–4087, doi:10.1128/aem.70.7.4079-4087.2004

Claustre, H., A. Bricaud, M. Babin, F. Bruyant, L. Guillou, F. Le Gall, D. Marie, and F. Partensky. 2002. Diel variations in *Prochlorococcus* optical properties. Limnol. Oceanogr. **47:** 1637–1647, doi:10.4319/lo.2002.47.6.1637

———, Y. Huot, I. Obernosterer, B. Gentili, D. Tailliez, and M. Lewis. 2008. Gross community production and metabolic balance in the South Pacific Gyre, using a non intrusive bio-optical method. Biogeoscience **5:** 463–474, doi:10.5194/bg-5-463-2008

———, A. Morel, M. Babin, C. Cailliau, D. Marie, J. C. Marty, D. Tailliez, and D. Vaulot. 1999. Variability in particle attenuation and chlorophyll fluorescence in the tropical Pacific: Scales, patterns, and biogeochemical implications. J. Geophys. Res. Oceans **104:** 3401–3422, doi:10.1029/98jc01334

———, and others. 2010. Guidelines towards an integrated ocean observation system for ecosystems and biogeochemical cycles. *In* J. Hall, D. E. Harrison, and D. Stammer [eds.], OceanObs'09: Sustained ocean observations and information for society (Vol. 1). ESA.

Cullen, J. J., M. R. Lewis, C. O. Davis, and R. T. Barber. 1992. Photosynthetic characteristics and estimated growth rates indicating grazing is the proximate control of primary production in the Equatorial Pacific. J. Geophys. Res. Oceans **97:** 639–654, doi:10.1029/91jc01320

Dall'Olmo, G., E. Boss, M. J. Behrenfeld, and T. K. Westberry. 2012. Particulate optical scattering coefficients along an Atlantic Meridional Transect. Opt. Express **20:** 21532–21551, doi:10.1364/OE.20.021532

———, T. K. Westberry, M. J. Behrenfeld, E. Boss, and W. H. Slade. 2009. Significant contribution of large particles to optical backscattering in the open ocean. Biogeosciences **6:** 947–967, doi:10.5194/bg-6-947-2009

D'Ortenzio, F., and M. Ribera d'Alcalà. 2009. On the trophic regimes of the Mediterranean Sea: A satellite analysis. Biogeosciences **6:** 139–148, doi:10.5194/bg-6-139-2009

Fennel, K., and E. Boss. 2003. Subsurface maxima of phytoplankton and chlorophyll: Steady-state solutions from a simple model. Limnol. Oceanogr. **48:** 1521–1534, doi:10.4319/lo.2003.48.4.1521

Gardner, W. D., A. Mishonov, and M. J. Richardson. 2006. Global POC concentrations from in-situ and satellite data. Deep-Sea Res. II **53:** 718–740, doi:10.1016/j.dsr2.2006.01.029

Gasol, J. M., M. D. Doval, J. Pinhassi, J. I. Calderon-Paz, N. Guixa-Boixareu, D. Vaque, and C. Pedros-Alio. 1998. Diel variations in bacterial heterotrophic activity and growth in the northwestern Mediterranean Sea. Mar. Ecol.-Prog. Ser. **164:** 107–124, doi:10.3354/meps164107

Gernez, P., D. Antoine, and Y. Huot. 2011. Diel cycles of the particulate beam attenuation coefficient under varying trophic conditions in the northwestern Mediterranean Sea: Observations and modeling. Limnol. Oceanogr. **56:** 17–36, doi:10.4319/lo.2011.56.1.0017

Gregg, W. W., and K. L. Carder. 1990. A simple spectral solar irradiance model for cloudless maritime atmospheres. Limnol. Oceanogr. **35:** 1657–1675, doi:10.4319/lo.1990.35.8.1657

Harding, L. W., B. W. Meeson, B. B. Prezelin, and B. M. Sweeney. 1981. Diel periodicity of photosynthesis in marine phytoplankton. Mar. Biol. **61:** 95–105, doi:10.1007/bf00386649

Huot, Y., A. Morel, M. S. Twardowski, D. Stramski, and R. A. Reynolds. 2008. Particle optical backscattering along a chlorophyll gradient in the upper layer of the eastern South Pacific Ocean. Biogeosci. **5:** 495–507, doi:10.5194/bg-5-495-2008

Kheireddine, M., and D. Antoine. 2014. Diel variability of the beam attenuation and backscattering coefficients in the northwestern Mediterranean Sea (BOUSSOLE site). J. Geophys. Res. Oceans **119:** 5465–5482, doi:10.1002/2014JC010007

Kuiper, N. H. 1960. Tests concerning random points on a circle. Proc. Koninkl. Neder. Akad. van Wetenschappen **63:** 38–47.

Levitus, S. 1982. Climatological atlas of the World Ocean. NOAA Professional Paper. U.S. Department of Commerce.

Loisel, H., E. Bosc, D. Stramski, K. Oubelkheir, and P. Y. Deschamps. 2001. Seasonal variability of the backscattering coefficient in the Mediterranean Sea based on satellite SeaWiFS imagery. Geophys. Res. Lett. **28:** 4203–4206, doi:10.1029/2001gl013863

———, X. Meriaux, J-F. Berthon, and A. Poteau. 2007. Investigation of the optical backscattering to scattering ratio of marine particles in relation to their biogeochemical composition in the eastern English Channel and southern North Sea. Limnol. Oceanogr. **52:** 739–752, doi:10.4319/lo.2007.52.2.0739

———, and A. Morel. 1998. Light scattering and chlorophyll concentration in case 1 waters: A reexamination. Limnol. Oceanogr. **43:** 847–858, doi:10.4319/lo.1998.43.5.0847

———, and others. 2011. Characterization of the bio-optical anomaly and diurnal variability of particulate matter, as seen from scattering and backscattering coefficients, in ultra-oligotrophic eddies of the Mediterranean Sea. Biogeosciences **8:** 3295–3317, doi:10.5194/bg-8-3295-2011

Maffione, R. A., and D. R. Dana. 1997. Instruments and methods for measuring the backward-scattering coefficient of ocean waters. Appl. Optics **36:** 6057–6067, doi:10.1364/ao.36.006057

Marra, J. 1997. Analysis of diel variability in chlorophyll fluorescence. J. Mar. Res. **55:** 767–784, doi:10.1357/0022240973224274

———, C. C. Trees, and J. E. O'Reilly. 2007. Phytoplankton absorption: A strong indicator of primary productivity in the surface ocean. Deep-Sea Res. I **54:** 155–163, doi:10.1016/j.dsr.2006.12.001

Martinez, E., D. Antoine, F. D'Ortenzio, and B. Gentili. 2009. Climate-driven basin-scale decadal oscillations of oceanic phytoplankton. Science **326:** 1253–1256, doi:10.1126/science.1177012

Martinez-Vicente, V., G. H. Tilstone, S. Sathyendranath, P. I. Miller, and S. B. Groom. 2012. Contributions of phytoplankton and bacteria to the optical backscattering coefficient over the Mid-Atlantic Ridge. Mar. Ecol.-Prog. Ser. **445:** 37–51, doi:10.3354/meps09388

Marty, J. C., and J. Chiaverini. 2002. Seasonal and interannual variations in phytoplankton production at DYFAMED time-series station, northwestern Mediterranean Sea. Deep-Sea Res. II **49:** 2017–2030, doi:10.1016/s0967-0645(02)00025-5

Mével, G., M. Vernet, M. Goutx, and J. F. Ghiglione. 2008. Seasonal to hour variation scales in abundance and production of total and particle-attached bacteria in the open NW Mediterranean Sea (0–1000 m). Biogeosciences **5:** 1573–1586, doi:10.5194/bg-5-1573-2008

Montes-Hugo, M. A., H. Ducklow, and O. M. Schoffeld. 2009. Contribution by different marine bacterial communities to particulate beam attenuation. Mar. Ecol.-Prog. Ser. **379:** 13–22, doi:10.3354/meps07883

Morel, A. 1991. Light and marine photosynthesis—a spectral model with geochemical and climatological implications. Prog. Oceanogr. **26:** 263–306, doi:10.1016/0079-6611(91)90004-6

———, D. Antoine, M. Babin, and Y. Dandonneau. 1996. Measured and modeled primary production in the Northeast Atlantic (EUMELI JGOFS program): The impact of natural variations in photosynthetic parameters on model predictive skill. Deep-Sea Res I **43:** 1273–1304, doi:10.1016/0967-0637(96)00059-3

———, and J.-F. Berthon. 1989. Surface pigments, algal biomass profiles, and potential production of the euphotic layer: Relationships reinvestigated in view of remote-sensing applications. Limnol. Oceanogr. **34:** 1545–1562, doi:10.4319/lo.1989.34.8.1545

———, B. Gentili, M. Chami, and J. Ras. 2006. Bio-optical properties of high chlorophyll Case 1 waters and of yellow-substance-dominated Case 2 waters. Deep-Sea Res. I **53:** 1439–1459, doi:10.1016/j.dsr.2006.07.007

Oubelkheir, K. J., H. Claustre, A. Sciandra, and M. Babin. 2005. Bio-optical and biogeochemical properties of different trophic regimes in oceanic waters. Limnol. Oceanogr. **50:** 1795–1809, doi:10.4319/lo.2005.50.6.1795

———, and A. Sciandra. 2008. Diel variations in particle stocks in the oligotrophic waters of the Ionian Sea (Mediterranean). J. Mar. Syst. **74:** 364–371, doi:10.1016/j.jmarsys.2008.02.008

Prezelin, B. B. 1992. Diel periodicity in phytoplankton productivity. Hydrobiologia **238:** 1–35, doi:10.1007/bf00048771

Ras, J., H. Claustre, and J. Uitz. 2008. Spatial variability of phytoplankton pigment distributions in the Subtropical South Pacific Ocean: Comparison between in situ and predicted data. Biogeosci. **5:** 353–369, doi:10.5194/bg-5-353-2008

Reynolds, R. A., D. Stramski, V. M. Wright, and S. B. Wozniak. 2010. Measurements and characterization of particle size distribution in coastal waters. J. Geophys. Res. **115:** C08024, doi:10.1029/2009JC005930

Siegel, D. A., T. D. Dickey, L. Washburn, M. K. Hamilton, and B. G. Mitchell. 1989. Optical determination of particulate abundance and production variations in the oligotrophic ocean. Deep-Sea Res. **36:** 211–222, doi:10.1016/0198-0149(89)90134-9

Sosik, H. M. 2008. Characterizing seawater constituents from optical properties, p. 281–329. *In* M. Babin, C. S. Roesler, and J. J. Cullen [eds.], Real-time coastal observing systems for ecosystem dynamics and harmful algal blooms: Theory, instrumentation and modelling. Oceanographic Methodology Series. UNESCO.

———, and R. J. Olson. 2007. Automated taxonomic classification of phytoplankton sampled with imaging-in-flow cytometry. Limnol. Oceanogr.: Methods **5:** 204–216, doi:10.4319/lom.2007.5.204

Stramska, M., and D. Stramski. 2005. Variability of particulate organic carbon concentration in the north polar Atlantic based on ocean color observations with sea-viewing wide field-of-view sensor (SeaWiFS). J. Geophys. Res. Oceans **110:** 16, doi:10.1029/2004jc002762

———, ———, R. Hapter, S. Kaczmarek, and J. Ston. 2003. Bio-optical relationships and ocean color algorithms for the north polar region of the Atlantic. J. Geophys. Res. Oceans **108:** 16, doi:10.1029/2001jc001195

Stramski, D., E. Boss, D. Bogucki, and K. J. Voss. 2004. The role of seawater constituents in light backscattering in the ocean. Prog. Oceanogr. **61:** 27–56, doi:10.1016/j.pocean.2004.07.001

———, and D. A. Kiefer. 1991. Light scattering by microorganisms in the open ocean. Prog. Oceanogr. **28:** 343–383, doi:10.1016/0079-6611(91)90032-h

———, and R. A. Reynolds. 1993. Diel variations in the optical properties of a marine diatom. Limnol. Oceanogr. **38:** 1347–1364, doi:10.4319/lo.1993.38.7.1347

———, ———, M. Kahru, and B. G. Mitchell. 1999. Estimation of particulate organic carbon in the ocean from satellite remote sensing. Science **285:** 239–242, doi:10.1126/science.285.5425.239

———, and others. 2008. Relationships between the surface concentration of particulate organic carbon and optical properties in the eastern South Pacific and eastern Atlantic Oceans. Biogeosciences **5:** 171–201, doi:10.5194/bg-5-171-2008

Vaillancourt, R. D., C. W. Brown, R. R. L. Guillard, and W. M. Balch. 2004. Light backscattering properties of marine phytoplankton: Relationships to cell size, chemical composition and taxonomy. J. Plankton Res. **26:** 191–212, doi:10.1093/plankt/fbh012

Vantrepotte, V., H. Loisel, F. Melin, D. Desailly, and L. Duforet-Gaurier. 2011. Global particulate matter pool temporal variability over the SeaWiFS period (1997–2007). Geophys. Res. Lett. **38:** 5, doi:10.1029/2010gl046167

Vaulot, D., and S. W. Chisholm. 1987. A simple model of the growth of phytoplankton populations in light dark cycles. J. Plankton Res. **9:** 345–366, doi:10.1093/plankt/9.2.345

Welschmeyer, N. A., A. E. Copping, M. Vernet, and C. J. Lorenzen. 1984. Diel fluctuation in zooplankton grazing rates as determined from the downward vertical flux of phaeopigments. Mar. Biol. **83:** 263–270, doi:10.1007/BF00397458

Westberry, T. K., G. Dall'Olmo, E. Boss, M. J. Behrenfeld, and T. Moutin. 2010. Coherence of particulate beam attenuation and backscattering coefficients in diverse open ocean environments. Opt. Express **18:** 15419–15425, doi:10.1364/OE.18.015419

Whitmire, A. L., W. S. Pegau, L. Karp-Boss, E. Boss, and T. J. Cowles. 2010. Spectral backscattering properties of marine phytoplankton cultures. Opt. Express **18:** 15073–15093, doi:10.1364/OE.18.015073

Zhang, X. D., L. B. Hu, and M. X. He. 2009. Scattering by pure seawater: Effect of salinity. Opt. Express **17:** 5698–5710, doi:10.1364/OE.17.005698

Associate editor: Heidi M. Sosik

Received: 10 February 2014
Accepted: 26 August 2014
Amended: 28 August 2014